Novel Sustainable Carbon Dot as Dual Replacements for Emulsion Stabilizers and Photoinitiators in Macroporous Polymerized High Internal Phase Emulsion Fabrication

Woming Gao[1]*, Zeming Cheng[1,2], Nicholas T.H. Farr[1,2], Cornelia Rodenburg[1,2]*, Frederik Claeyssens[1,2]*
* Corresponding authors

[1] School of Chemical, Materials and Biological Engineering, Sir Robert Hadfield Building, University of Sheffield, Sheffield, S1 3JD, UK
[2] Insigneo Institute for in Silico Medicine, Pam Liversidge Building, University of Sheffield, S1 3JD, UK

Keywords: carbon dots; emulsion stabilizer; photoinitiator; macroporous PolyHIPEs; enlarged pore throats; fluid permeability; cell permeability

Abstract

Both emulsion stabilizers and photoinitiators are essential components in preparing photocurable water-in-oil (w/o) Polymerized High Internal Phase Emulsions (PolyHIPEs). Conventional stabilizers like Hypermer B246 and photoinitiators like 2,4,6-Trimethylbenzoyldiphenylphosphine oxide (TPO) pose environmental and biological hazards, requiring careful removal before use in bioengineering applications. Furthermore, PolyHIPEs prepared with traditional surfactants often feature narrow pores and pore throats, limiting effective fluid and cell infiltration. As a class of easy-synthesizing and biocompatible nanoparticles, carbon dots (CDs) exhibit potential for use as emulsion stabilizers and photoinitiators. Herein, novel amphiphilic carbon dots (GW CDs) were synthesized from Gromwell root waste, a byproduct of shikonin extraction, as sustainable alternative. GW CDs demonstrated excellent emulsion-stabilizing ability, effective photoinitiating performance and superior biocompatibility. GW CDs were employed to stabilize the emulsions and successfully crosslink them under UV light to fabricate 2-ethylhexyl acrylate (EHA)- isobornyl acrylate (IBOA)-trimethylolpropane triacrylate (TMPTA) PolyHIPEs. The pore size and pore throat formation of the resulting PolyHIPEs could be effectively tuned by adjusting the GW CDs content. Compared to PolyHIPEs prepared using Hypermer B246 and TPO, the GW CD-stabilized counterparts exhibited significantly larger pore sizes and pore throats, improving fluid and cell permeability for tissue engineering applications. Additionally, GW CDs possess upconversion luminescence, pH sensitivity, and cell-imaging capabilities, further highlighting their potential in biomedical engineering and environmental science applications.

1. Introduction

Polymerized High Internal Phase Emulsions (PolyHIPEs) are highly porous polymeric materials fabricated via emulsion templating methods. During fabrication, the polymerizable continuous phase cures to form a solid scaffold, while removal of the dispersed internal aqueous phase droplets results in the formation of a highly interconnected porous network [1]. Photocurable water-in-oil (w/o) high internal phase emulsions (HIPEs), such as the 2-ethylhexyl acrylate (EHA)- isobornyl acrylate (IBOA)- trimethylolpropane triacrylate (TMPTA) PolyHIPEs, are widely used due to their tunable mechanical properties and easy processing [2]. These PolyHIPEs have found applications in protein immobilization [3], bone tissue engineering scaffolds [4], and microfluidic osteogenesis platforms [5]. Their formulation typically requires both emulsion stabilizers and photoinitiators, commonly used examples include Hypermer B246 (Hypermer) as the emulsifier and 2,4,6-Trimethylbenzoyldiphenylphosphine oxide (TPO) as the photoinitiator. However, these additives often pose cytotoxicity and environmental concerns, their release into soil and water systems can lead to eutrophication and acidification, adversely affecting biological ecosystems [6], [7], [8], [9], [10]. Their incomplete removal during processing poses challenges for biomedical and environmental applications, particularly in tissue engineering [11], [12]. Additionally, emulsions stabilized with traditional surfactants often form PolyHIPEs with pore sizes among 1-50 microns and pore throats less than 10 microns, which can induce capillary effects due to surface tension, ultimately hindering fluid transport and cellular infiltration [13]. Therefore, the development of biocompatible, low-toxicity alternatives to conventional emulsifiers and photoinitiators is critical for the fabrication of macroporous PolyHIPEs with enlarged pore throats.

In this study, we aimed to prepare a novel and sustainable carbon dot (CD) as the alternative. CDs are a class of zero-dimensional carbon nanomaterial with excellent biocompatibility, low cost and outstanding optical properties [14], [15], [16]. As solid nanoparticles, CDs can serve as stabilizers for Pickering emulsions [17]. By chemically modifying their surface functional groups to tune hydrophilicity and hydrophobicity, they can be irreversibly adsorbed at the oil-water interface, acting as a strong mechanical barrier to stabilize emulsion [18]. Moreover, certain modified groups on the surface of CDs can trigger photoinitiation by generating free radicals [19]. CDs based on natural sources typically exhibit low toxicity, making them green alternatives to conventional photoinitiators and surfactants [20]. To date, although few studies have reported the use of CDs or their derivatives as either emulsion stabilizers (Rong Ma, et al. [21]) or photoinitiators (Ruiping Li, et al. [19]), there have been no report of a single type of CDs simultaneously fulfilling both roles in the fabrication of PolyHIPEs. Furthermore, while Pickering emulsions are known to produce PolyHIPEs with larger pore sizes compared to those stabilized by traditional surfactants, they typically fail to generate sufficient pore throats between adjacent pores [22], [23]. Whether CDs can help to form the macroporous PolyHIPEs with enlarged pore throats remains to be investigated.

To address this, we repurposed hydrophobic gromwell root waste powder (GW), a byproduct of shikonin production, and dispersed it in acrylic acid. Using a microwave-assisted method, we successfully synthesised carbon dots from this mixture, referred to as GW-acrylic acid carbon dots (GW CDs). Their morphology, chemical structure, properties were comprehensively characterized to assess their potential as biocompatible emulsifiers and photoinitiators. GW CDs were then incorporated at various mass ratios into EHA-IBOA-TMPTA formulations to fabricate PolyHIPEs, which were systematically compared both among themselves and against PolyHIPEs prepared using conventional additives (Hypermer and TPO). The comparison focused on structural characteristics, particularly the formation and size of pores and pore throats, as well as the resulting improvements in the permeability of liquid and cells.

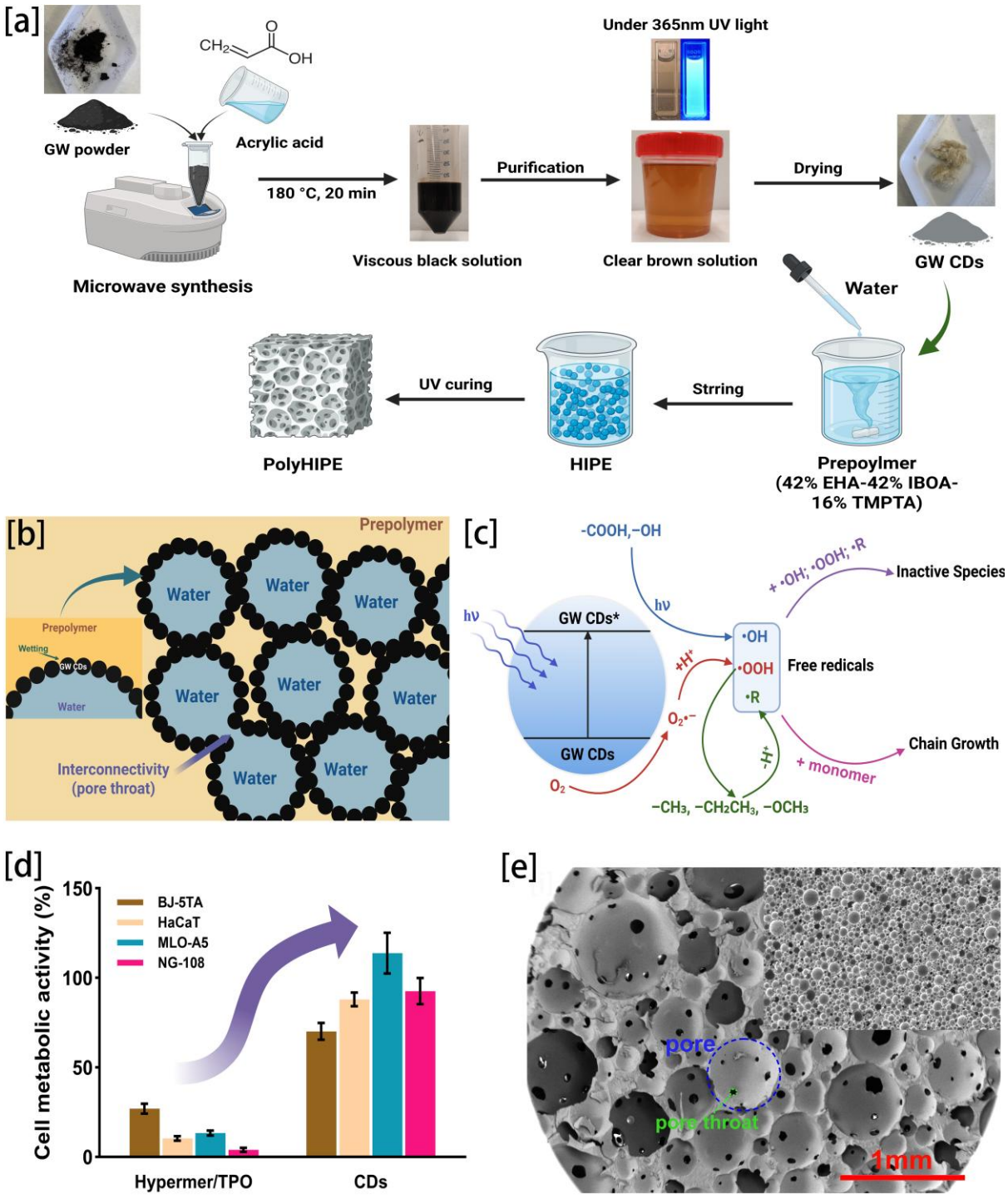

Figure 1. (a) Schematic diagram of the synthesis and purification of GW CDs, followed by the preparation of GW CDs/EHA-IBOA-TMPTA PolyHIPEs. (b) Possible mechanism of GW CDs as Pickering emulsion stabilizers for PolyHIPEs. (c) Possible mechanism of GW CDs as photoinitiator. (d) Cell viability assays demonstrated that GW CDs exhibited superior biocompatibility compared to conventional additives such as Hypermer B246 and TPO. (e) SEM images of PolyHIPEs prepared using GW CDs and Hypermer (inset image) at the same concentration (4 wt%) reveal that the GW CDs-stabilized PolyHIPE exhibits significantly larger pore size（blue circle） and pore throat diameters (green circle) compared to the Hypermer-based counterpart (inset image), two image are with the same scale bar (1 mm).

2. Results and Discussion

2.1 Potential of GW CDs as biocompatible emulsion stabilizers and photoinitiator

Shikonin was extracted from the Gromwell root powder, leaving behind GW (Figure 1a). GW was mixed with acrylic acid and subjected to microwave heating at 180 °C for 20 minutes After purification and drying, light grey flocculent GW CDs were obtained (Figure 1a). The aqueous solution of CDs showed bright blue-green fluorescence under 365 nm ultraviolet light (inset of Figure 1a). This synthesis was repeated three times, and the resulting batches showed nearly identical Fourier Transform Infrared Spectroscopy (FTIR), ^{1}H Nuclear Magnetic Resonance (NMR) and photoluminescence (PL) emission spectra (Figure S17), confirming good batch-to-batch reproducibility and consistent surface functionalization of the GW CDs.

The potential of GW CDs as both Pickering emulsion stabilizers and photoinitiators was demonstrated through comprehensive morphological and chemical characterizations. Transmission electron microscopy (TEM) revealed that GW CDs are spherical nanoparticles with a uniform size distribution in the range of 1-3 nm (Figure 2a). High-resolution transmission electron microscopy (HRTEM) image of individual GW CDs reveal distinct lattice fringes with interplanar spacing of 0.21 nm (Figure 2b), which indicated an ordered graphitic layer structure [24], [25]. The broad diffraction peaks centered around 20° (002) and 40° (100) in the X-ray diffraction (XRD) spectrum (Figure 2c) and the sharp weight loss observed between 400 °C and 500 °C in the thermogravimetric analysis (TGA) (Figure S2) also confirmed that GW CDs possessed a graphitized, sp^2-conjugated core [26], [27]. This rigid, solid carbon core that imparted high structural integrity, enabling the GW CDs to better resist destabilizing forces such as Brownian motion, gravitational separation, and shear stress, which promoted droplet coalescence or phase separation in emulsions [28].

Furthermore, the surface chemistry of GW CDs played a vital role in emulsion stabilization and photoinitiation. FTIR, NMR and X-ray Photoelectron Spectroscopy (XPS) confirmed that GW CDs retained the elemental diversity of their natural GW and acrylic acid precursor (C, H, O, N, K, Ca) (Figure 2e) as well as inherited various hydrophobic and hydrophilic surface groups. The presence of aliphatic and aromatic hydrophobic domains is evidenced by C-H stretching and bending bands and C=C stretching in FTIR, sp^2/sp^3 carbon and π-π* satellite features in the C1s XPS spectrum, and $^{1}H/^{13}C$ NMR signals in the 1-3 ppm and 1-50 / 100-160 ppm regions, respectively (Figure 2d,f-h) [29], [30], [31], [32]. Hydrophilic functionalities, including hydroxyl, carboxyl and C-O/C-N groups, are indicated by the broad O-H and C=O bands in FTIR, the corresponding C-O/C-N/C=O components in C1s and O1s XPS, and $^{1}H/^{13}C$ NMR resonances at 3.5-5.0 ppm and 50-100 / 170-200 ppm. [33], [34], [35], [36]. Table S2 summarized the comparative elemental composition and groups percentage of GW CDs and GW by XPS. These diverse surface functionalities modulated the overall

amphiphilicity of GW CDs, which was further supported by wettability measurements, showing a water contact angle of ~90.7° for GW CDs coated on glass (Figure 2i), which confirmed the amphiphilic characteristic. Amphiphilic surface groups enabled GW CDs to be wetted by both aqueous and oil phases, facilitating their migration to the oil-water interface and forming a steric barrier to stabilize emulsions [2]. Additionally, surface groups such as hydroxyl, carboxyl, amine, and aliphatic chains, could facilitate electron or energy transfer processes, which promoted photo-crosslinking by generating radicals.

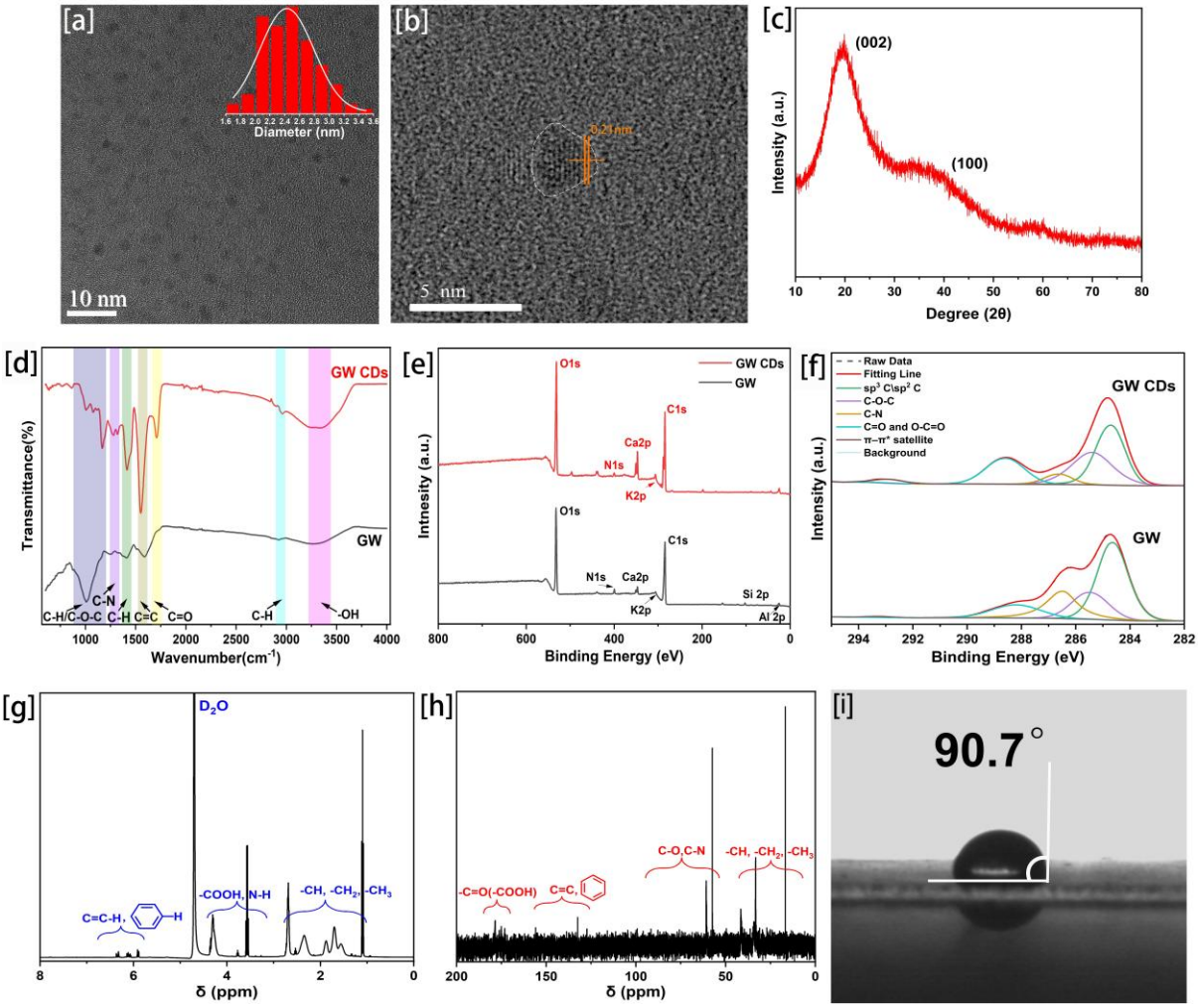

Figure 2. TEM image (a) of GW CDs with a scale bar of 10 nm. Inset: the corresponding particle size histogram, the particle size distribution of no less than 100 particles was measured. HRTEM image (b) of a single GW CD with a scale bar of 5 nm. The XRD spectrum (c) of GW CDs. FTIR (d), the full XPS survey (e) and high-resolution C1s XPS spectra (f) of GW and GW CDs. The ^{1}H-NMR (g) and ^{13}C-NMR spectra (h) of GW CDs recorded in D_2O. (i) The morphology and contact angle of deionized water droplets on GW CDs film covered on a glass slide.

While morphological and chemical characterizations suggested the strong potential of GW CDs being a replacement for Pickering emulsion stabilizers and photoinitiators, experimental validation is essential to confirm their functional performance. In the IBOA-EHA-TMPTA w/o emulsion, the oil was the continuous external phase, and the

water droplets were dispersed internal phase. Therefore, in order to stabilize the emulsion, GW CDs need to be oil-biased with a hydrophilic-lipophilic balance (HLB) of 3-8 [37], [38]. The HLB of GW CDs was calculated based on the ^{1}H NMR spectrum integration, and the calculated result was 7.39 (Figure S4 and Table S3), which was within the range. Because GW CDs are structurally heterogeneous, this value should be regarded as a semi-quantitative indicator of amphiphilicity rather than a conventional surfactant HLB, but it is consistent with their experimentally observed ability to stabilize w/o emulsions. To determine the effective dosage for micellization and emulsion stabilization, the critical micelle concentration (CMC) of GW CDs was measured by fluorescent spectrometry and the result was ~400 mg/L (Figure 3a), indicating that for an emulsion containing 80 vol% water, the minimum concentration of GW CDs in the organic phase should reach ~0.2 wt% for a stable micelle formation.

As potential photoinitiator, GW CDs must be able to absorb UV light and facilitate energy transfer. UV-vis spectrum and fluorescence emission spectrum (Figure 3b) showed the absorption peaks at 318 nm and 346 nm and emission peaks at 398 and 438 nm upon excitation at 345 nm. Additionally, the Excitation-Emission Matrix (EEM) (Figure 3c) with Rayleigh and Raman scattering removed revealed a broad absorption and emission range (300-600 nm), indicating that multiple emissive centres and efficient energy transfer pathways, confirming their ability of UV absorption and energy conversion. However, if too much energy was dissipated via fluorescence, the efficiency of radical generation could be compromised [39],[40]. Positively, the photoluminescence quantum yield (PLQY) of GW CDs was 28.33%, which was moderate for effective light harvesting without excessive energy loss in fluorescence (Figure S6). Comparing the PL intensity of GW CDs in water and in prepolymer solution (42% EHA, 42% IBOA and 16% TMPTA), it was found that the GW CDs underwent fluorescence quenching in prepolymer solution, which demonstrated certain amount of energy transfer to the prepolymer (Figure 3d). Also to explore excited-state interactions with the prepolymer, we performed steady-state PL quenching experiments using the prepolymer and analysed the results with Stern-Volmer plots. Fluorescence spectra of GW CDs and, for comparison, TPO were recorded in ethanol under 365 nm excitation while gradually increasing the prepolymer concentration (0-100 mM), ensuring all solutions had low absorbance (≤ 0.2) to minimize inner filter effects. The Stern-Volmer plots (Figure S16) owed linear relationships between the fluorescence quenching ratio (I_0/I) and monomer concentration, consistent with dynamic quenching. The fitted Stern-Volmer constants were K_{SV} = 12.6 M^{-1} for GW CDs and K_{SV} = 20.2 M^{-1} for TPO, indicating that GW CDs engage in monomer interactions at a similar efficiency to commercial photoinitiators.

To assess the radical-generating potential of GW CDs, their structural stability under UV irradiation was examined. No significant structural changes in GW CDs were found from the TEM and XRD analyses, which indicated the intact remaining of carbon core (Figures S7 and S8). FTIR spectra revealed the signal change of C=O and -OH signals within various exposure time, suggesting the possibility of CDs undergoing loss of functional groups or chemical transformation upon UV irradiation (Figure 3f). Electron Paramagnetic Resonance (EPR) spectroscopy using 5,5-Dimethyl-1-pyrroline N-oxide

(DMPO) as a spin trap confirmed the radical formation. In the dark, GW CDs generated carbon-centered radicals (DMPO-•R) and hydroperoxyl radicals (DMPO-•OOH) [41], [42]. Upon UV exposure, strong Hydroxyl radicals (DMPO-•OH) signals were also observed alongside the previous radicals (Figure 3e) [43]. Simulated EPR spectra corresponded to experimental data (Figure S9a). The DMPO-•OOH could be formed because the electrons were transferred to the dissolved oxygen-generated superoxide radicals ($•O_2^-$) and got them protonated [44]. The •OOH radicals could subsequently oxidize methyl groups on GW CDs, withdrawing proton from the methyl groups, leading to the formation of •R radicals [45]. The above mechanism was confirmed by the absence of both DMPO-•OOH and DMPO-•R EPR signals in the deoxygenated system in the dark (Deoxygenated water was prepared by boiling deionized water and then purging with Nitrogen). Conversely, strong DMPO-•OH signals were still detected in the deoxygenated system under UV light, indicating that the photoexcitation of -OH and -COOH groups may drive •OH formation (Figure S9b) [43], [46]. More •OH was found to be constantly generated with continuous UV irradiation, demonstrating the sustained photoinitiation capability of CDs. With strong reactivity, •OH could effectively attack C=C double bonds and initiate free-radical polymerization [47], [48], [49].

Supported by above analyses, a possible mechanism for GW CDs in Pickering emulsion stabilization and photoinitiation was proposed (Figures 1b and 1c).

GW CDs also demonstrated excellent biocompatibility. Four different cell lines (BJ-5TA, HaCaT, MLO-A5, and NG-108) were cultured in blank media, media supplemented with GW CDs (1000 mg/L), and media containing Hypermer/TPO at the same concentration, followed by the assessment of cell viability (Figure 3g). In comparison to cells in normal blank media (positive control), all cell lines supplemented with GW CDs showed metabolic activity higher than 70% (BJ5TA: 72.12%, HaCaT: 87.96%, MLO-A5: 113.80%, NG-108: 92.62%), which proved that GW CDs were non-cytotoxic according to ISO 10993-5 standards [50]. By contrast, the viability of cells cultured in Hypermer/TPO supplemented media was drastically decreased (BJ-5TA: 26.94%, HaCaT: 10.33%, MLO-A5: 13.31%, NG-108: 3.99%). Figures 4h and 4i presented the morphology of NG-108 cells in media containing GW CDs and Hypermer/TPO after 24-hour culture respectively. The cells in GW CDs group exhibited healthy, plump shape with clear cell membrane boundaries and stretched pseudopods, whereas the cells in Hypermer/TPO group exhibited severe shrinkage, blurred boundaries, and apparent membrane degradation. The phenomenon of healthy cells in GW CDs group and damaged cells in Hypermer/TPO group also applied to the rest cell lines (Figure S10). Both the results cell viability and cell morphology presented the excellent biocompatibility of GW CDs and revealed the pronounced cytotoxicity of Hypermer and TPO, highlighting the potential of GW CDs as a green alternative to traditional emulsion stabilizers and photoinitiators.

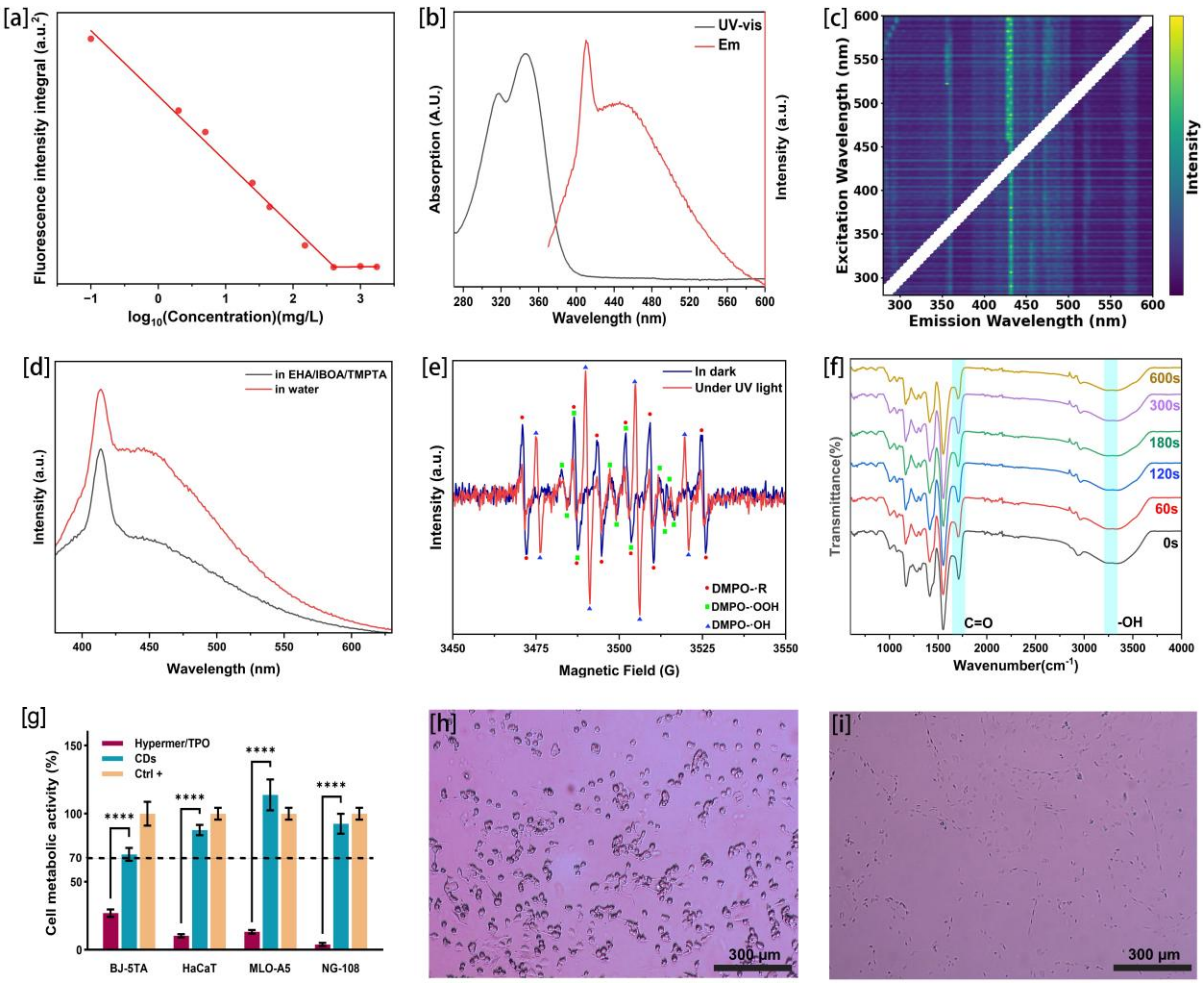

Figure 3. (a) The CMC of GW CDs. (b) The absorption and emission curves of GW CDs. (c) The EEM of GW CDs, with Rayleigh and Raman scattering removed. (d) Fluorescence emission intensities of GW CDs (0.05 g/L) in water and in prepolymer under 350 nm UV light. (e) EPR spectra of radicals formed from GW CDs both in the dark and under UV irradiation. (f) FTIR spectra of GW CDs upon UV irradiation with different exposure time. (g) The cell metabolic activity of BJ-5TA, HaCaT, MLO-A5, and NG-108 in blank media, media supplemented with GW CDs (1000 mg/L), and media containing Hypermer/TPO at the same concentration. The morphology of NG-108 cells in media containing GW CDs (h) and Hypermer/TPO (i) with scale bars of 300 μm.

2.2 Photocurable EHA-IBOA-TMPTA PolyHIPE with GW CDs

Motivated by the promising capabilities of GW CDs in emulsion stabilization, photoinitiation, and biocompatibility, we incorporated them into the synthesis of PolyHIPEs at varying mass ratios (1 wt%, 2 wt%, 4 wt%, 6 wt% to 14 wt%). For comparison, a control PolyHIPE was prepared using 4 wt% Hypermer as the surfactant and TPO as the photoinitiator. Detailed formulations of all PolyHIPEs were listed in Table S1. Emulsions containing different concentrations of GW CDs were successfully stabilized and subsequently crosslinked, demonstrating that GW CDs can function effectively as both emulsion stabilizers and photoinitiators. Quantitative

evaluation of gelation time and gel fraction using vial inversion experiments (Figure 4c) showed that increasing the GW CDs content led to a progressive decrease in gelation time, from 248 ± 23 s at 1 wt% to 66.7 ± 10.4 s at 14 wt%, and a corresponding increase in gel fraction, from 76 ± 7% to 90 ± 1%. These values closely approach those of the TPO control groups (2 wt% and 5 wt%), which exhibited gel times of 66.7 ± 2.9 s and 45.0 ± 5.0 s, and gel fractions of 82 ± 4% and 95 ± 3%, respectively. A comparison with the stability time of each emulsion before creaming and the long-term emulsion stability data (Figure S1b and S1c, Table S7) confirms that the emulsion remains stable well beyond the time required for curing. Emulsions prepared with low GW CDs content (1 to 4 wt%) exhibited rapid droplet coalescence, with average droplet diameters increasing to several hundred microns within 1 to 2 h, ultimately leading to phase separation (creaming). However, this timespan was still sufficient for successful photocuring. In contrast, formulations containing 6 to 8 wt% GW CDs maintained nearly constant droplet sizes for several hours to over a day. Notably, emulsions stabilized with 10 to 14 wt% GW CDs showed minimal change in average droplet diameter over a full 7-day period, indicating excellent long-term emulsion stability. Polymerization kinetics, evaluated by photo differential scanning calorimetry (photo-DSC) and time-resolved FTIR (Figure 4a, Table S6 shows photo-DSC data; Figure 4b shows time-resolved FTIR data), further confirmed that both the polymerization rate and extent increased significantly with higher GW CDs content. Time-resolved FTIR showed that the time required to reach 50% double bond conversion decreased from approximately 180 s at 1 wt% to approximately 10 to 15 s at 14 wt%. Moreover, when the GW CDs content exceeded 4 wt%, the final double bond conversion surpassed 88%, approaching the levels observed with TPO as the photoinitiator. Photo-DSC measurements showed that GW CDs produced broader and weaker exothermic peaks compared to TPO, although the peak intensity increased with higher GW CD concentrations. The total curing enthalpy (ΔH) (Table S6) also increased from approximately 4.02 J/g at 1 wt% to 5.16 J/g at 14 wt%, closely matching the performance of 2 and 5 wt% TPO (conversion: 91% and 94%, ΔH: 5.44 and 4.38 J/g). Figure 4 showed the SEM images of all GW CD-based PolyHIPEs, alongside the control sample. Two additional control experiments were conducted: (1) without GW CDs or Hypermer, the emulsion collapsed instantly (within 1 second) (Video S1); (2) without a photoinitiator, the emulsion remained stable but could not crosslink under UV irradiation (Video S2). These results confirmed GW CDs contributed to both stability and photopolymerization (Video S3 and S4).

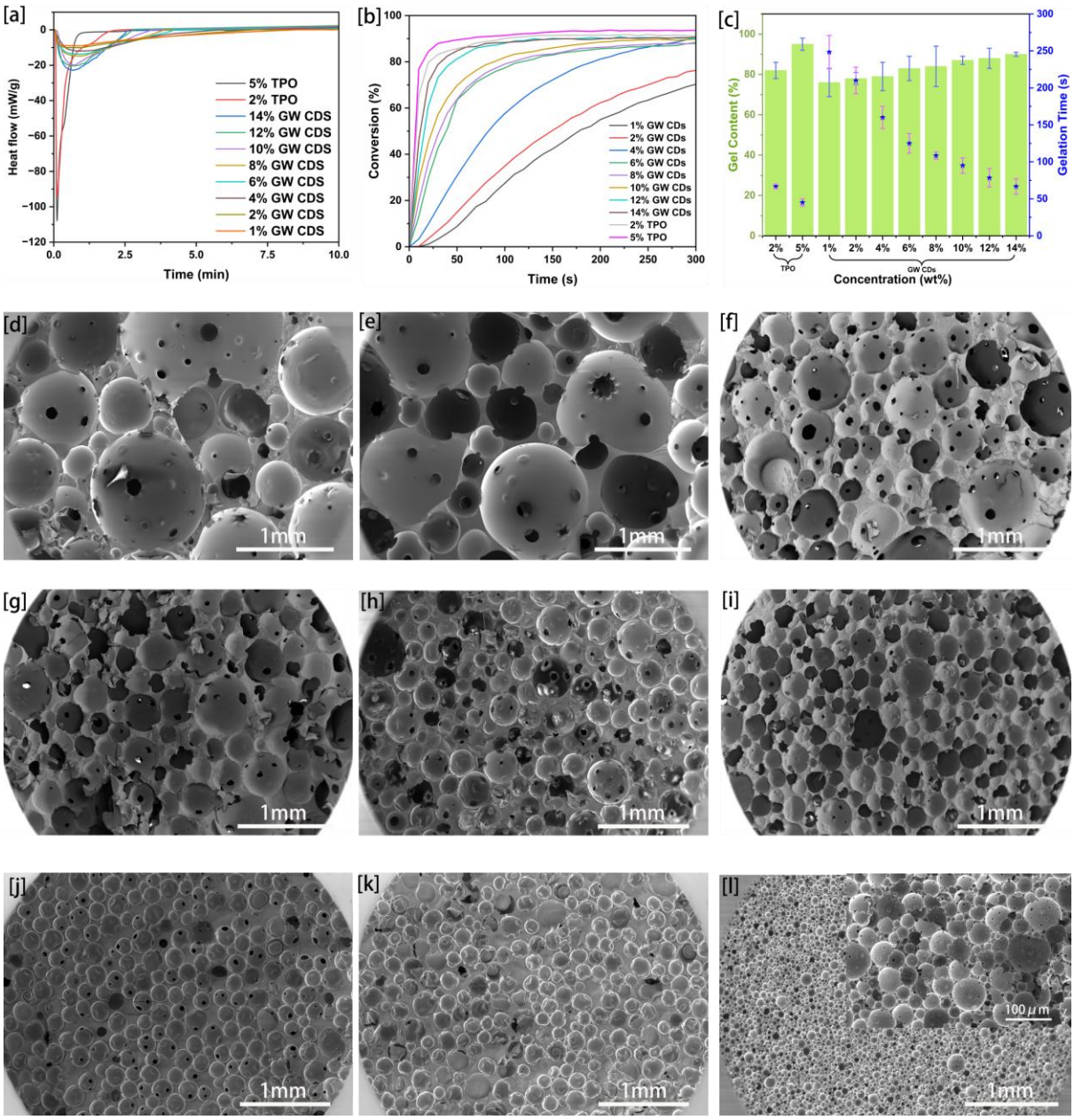

Figure 4. The Photo-DSC (a), the time-resolved FTIR (b) curves of prepolymer polymerization with different GW CDs or TPO concentrations, the gelation time and the gel content at this point of each emulsion (c) under 405 nm UV light, light intensity is 700 mW/cm². SEM images of PolyHIPE samples containing 1 wt% (d), 2 wt% (e), 4 wt% (f), 6 wt% (g), 8 wt% (h), 10 wt% (i), 12% wt% (j) and 14 wt% (k) GW CDs, as well as a control sample (l) prepared with the standard addition of 4% Hypermer and TPO. The scale bar from figure (d)-(k) is 1mm and inset image of (l) is 100 μm.

The average pore diameter, average number of pore throats per pore, and average pore throat diameter for the various PolyHIPE formulations were directly measured on SEM images were summarized in Figure 5a and detailed in Table S4. PolyHIPEs stabilized by GW CDs exhibited larger pore size than the PolyHIPE stabilized with Hypermer, and formed an interconnected macroporous structure. Notably, unlike the Hypermer-stabilized PolyHIPE whose pore size remained mostly unaffected by

changes in surfactant concentration (2 wt%, 4 wt%, 6 wt%, Figure S12), the average pore size of GW CDs-stabilized PolyHIPEs decreased with the increase of GW CDs proportion, indicating that content of the GW CDs can control the pore size. Even at the highest concentration (14 wt%), the resulting PolyHIPE still retained a considerably larger average pore size (144 ± 24 μm) than the sample stabilized by Hypermer (51 ± 8 μm).

The pore size of GW CDs-stabilized PolyHIPEs is influenced by both the concentration of carbon dots and the emulsion temperature. Static light scattering (SLS) measurements of emulsions at room temperature (20 °C) revealed that the resulting PolyHIPEs exhibited larger pore sizes (Figure 5a and Table S4) than the initial droplet diameters (Figure 5b and Table S5) prior to photocuring. This expansion was likely attributed to light absorption and exothermic reactions during polymerization which increased the emulsion temperature. Temperature measurements using a thermal probe indicated that the surface temperature of the PolyHIPEs reached around 66-73 °C after 180 seconds of curing under 365 nm UV light at an intensity of 1700 mW/cm^2 (Figure S13). The increased temperature enhanced water molecule mobility and promoted droplet coalescence, leading to larger droplet size and larger pores upon curing [51]. SLS was continuously used to assess the droplets diameters of emulsions incubated at 45 and 70 °C (Figure 5b and Table S5). The results confirmed a temperature-dependent increase in droplet size, and the droplet size at 80 °C turned out to be closer to the final pore size of the PolyHIPEs. Moreover, the impact of increased temperature on droplet size correlated negative with GW CD concentration, suggesting that higher interfacial accumulation of CDs improved emulsion stability by effectively inhibiting droplet coalescence and promoting smaller pore formation upon curing [52]. To directly probe the effect of GW CDs concentration on droplet coalescence, we conducted confocal fluorescence imaging of those PolyHIPEs. As shown in Figure 5c (14 wt% GW CDs) and Figure S15 (other concentrations), GW CDs were observed around the pores' surface, emitting bright fluorescence under UV light. This confirmed that GW CDs accumulated at the oil-water interface. Notably, both the intensity and continuity of the interfacial fluorescence increased with GW CDs content, suggesting the progressive formation of a denser and more uniform particulate layer at the interface. These observations are consistent with our previously conducted long-term emulsion stability experiments (Figure S1c), which demonstrated that emulsions with lower GW CDs content underwent more rapid increases in average droplet size during storage, indicative of substantial droplet coalescence. In contrast, formulations containing higher GW CDs loadings exhibited significantly improved emulsion stability, with negligible droplet growth over time. When combined with SEM-based quantitative analysis of the resulting pore size, throat diameter, and interconnectivity (Figure 5a and Table S4), these results support the following mechanistic interpretation: at low GW CDs concentrations, incomplete coverage of the droplet interface allows for thermally induced coalescence during UV curing, leading to the formation of larger pores and more abundant, wider throats. In contrast, higher GW CDs concentrations enable more complete interfacial coverage, suppressing coalescence and yielding PolyHIPEs with smaller pore sizes and

narrower, less frequent throats.

However, droplet coalescence during the curing process is beneficial for the formation of interconnected pores. Increased accumulation of CDs at the interface also results in a reduced number of pore throats per pore. Comparison of the high-magnification SEM images of 14 wt% GW CDs-stabilized PolyHIPE and Hypermer-stabilized PolyHIPE revealed distinct structural differences. While the Hypermer-stabilized sample displayed remarkable micron- and submicron-scale interconnected pore throats (Figure 5d), the 14 wt% GW CDs-PolyHIPE showed areas with visible CDs agglomerates (highlighted in blue square, Figure 5d) and regions where pore connections appeared to initiate but ultimately failed to form (highlighted in red square, Figure 5e). These observations supported the hypothesis that CDs aggregation at the interface stabilized emulsion droplets but impeded pore throats formation. The impact of temperature on pore size was minimised on emulsions containing 14 wt% CDs and resulted in PolyHIPEs with poor pore interconnectivity. In contrast, although emulsions with lower CDs content were less stable when temperature increased, larger and more interconnected pores were formed due to greater droplet coalescence during curing, which was desirable for the PolyHIPEs' applications requiring enhanced permeability and cellular infiltration. Hypermer-based samples featured narrow throats (3±2 μm) and small pores (51±8 μm), which were less favourable for fluid and cell infiltration due to enhanced capillary resistance. In contrast, although with fewer pore throats, GW CDs-stabilized scaffolds exhibited significantly larger pore throat diameters (e.g., 31±10 μm for 12 wt% GW CDs-stabilized PolyHIPE), which subsequently facilitated liquid and cell penetration. Liquid penetration tests (Figure 5f) demonstrated that GW CDs-stabilized PolyHIPEs exhibited faster fluid uptake and higher permeability correlating with larger pores and throats.

The confocal images of the cross-section of cell-seeded PolyHIPEs also proved that larger pores and throats helped cell infiltration. As shown in the image (Figure 5g and 5h), MDA-MB-231 cells (green fluorescence from GFP and red fluorescence from Phalloidin-TRITC) staining were obstructed at the outer surface of the Hypermer/TPO-PolyHIPEs without inward expansion. In comparison, the cells seeded on 12% GW CDs-stabilized PolyHIPEs were found not only growing on the scaffold outer surface but also migrating and proliferating inside the pores through the pore throats (As marked in the white circle in Figure 5g). Although the 12 wt% sample had fewer and narrower throats compared to formulations with lower GW CDs concentrations, its interconnectivity was still sufficient to support effective cell invasion. This observation suggests that samples with GW CDs concentrations below 12 wt% may exhibit even better permeability, as they typically possess more and larger interconnect pores. Nevertheless, the 12 wt% sample already provided adequate pore interconnectivity to enable robust cell infiltration. Compared with Hypermer/TPO-PolyHIPEs, 12 wt% GW CDs-PolyHIPEs had significantly bigger pores and pore throats, which enabled cells' migration and proliferation within the scaffolds.

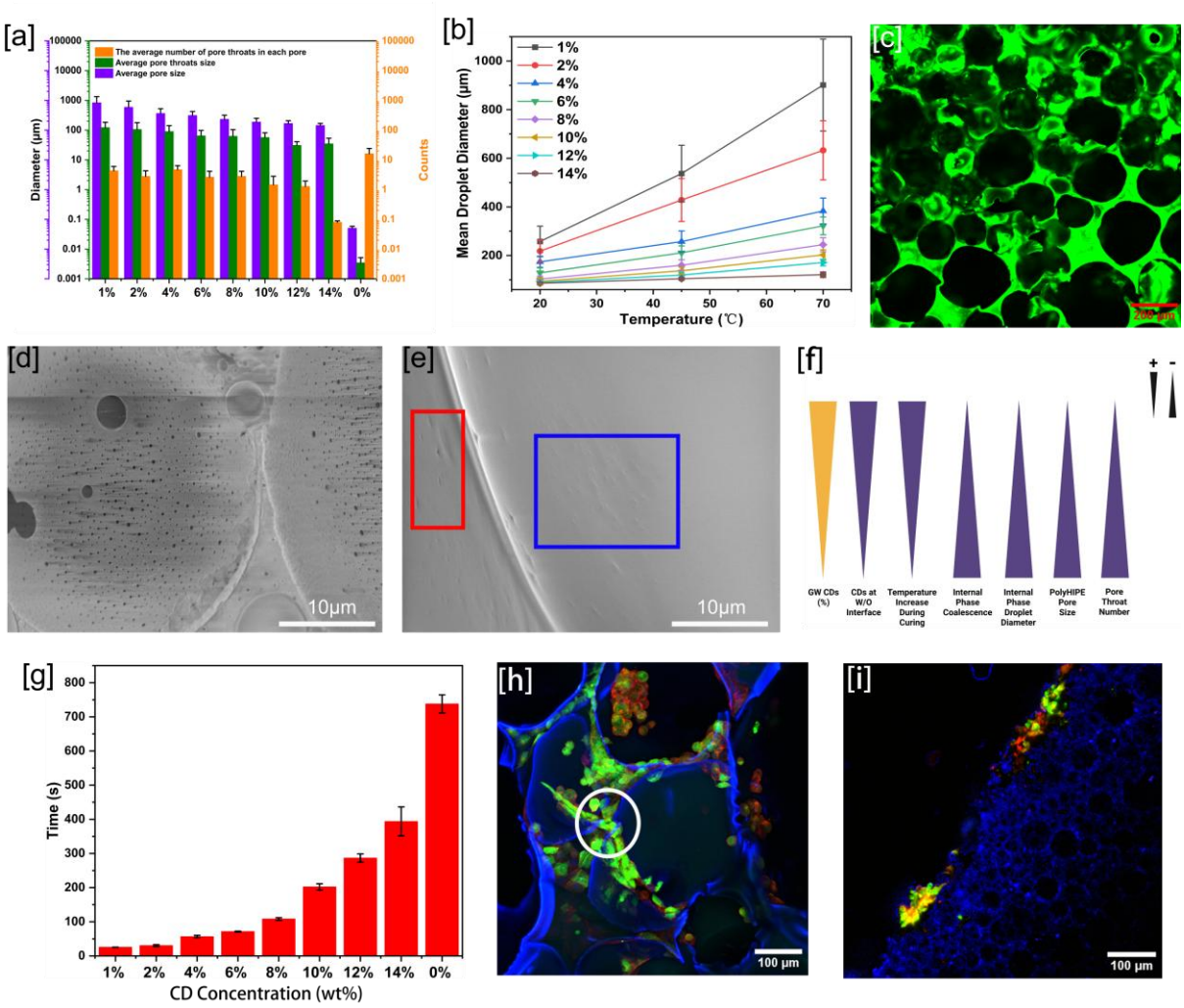

Figure 5. (a) Average pore size, number of pore throats per pore, and pore throat diameter for each PolyHIPE sample (n=100). (b) The average droplet size of each PolyHIPE emulsion under different temperatures. (c) The confocal image of 14 wt% GW CDs-PolyHIPE under 488 nm wavelength，the scale bar is 200 μm. The SEM image of Hypermer/TPO-PolyHIPE (d) and 14 wt% GW CDs-PolyHIPE (e), all the scale bars are 10 μm. (f) The summary of the effect of GW CDs content on pore and pore throat control. The inverted triangle (▼) indicates increase (+), while the upright triangle (▲) indicates decrease (−). (g) Liquid penetration time test results. (h)-(i) Confocal images of cell infiltration into 12 wt% PolyHIPEs.

2.3 Other potential applications of GW CDs

Apart from being a candidate of novel emulsion stabilizers and photoinitiators, GW CDs exhibited a range of promising properties suggesting their broader application potential. For instance, their distinct two-photon upconversion photoluminescence characteristics made them suitable candidates for photodynamic therapy and electrocatalysis (Figure 6a and Figure S18) [53]. Furthermore, GW CDs displayed multicolour fluorescence, enabling their potential usage in cellular multicolour imaging (Figure 6b). Additionally, they also turned out to be sensitive to pH changes, which might be leveraged for environmental sensing or biomedical diagnostics (Figure 6c

and 6d). Collectively, these features highlighted the substantial versatility and research value of GW CDs for future applications.

DE

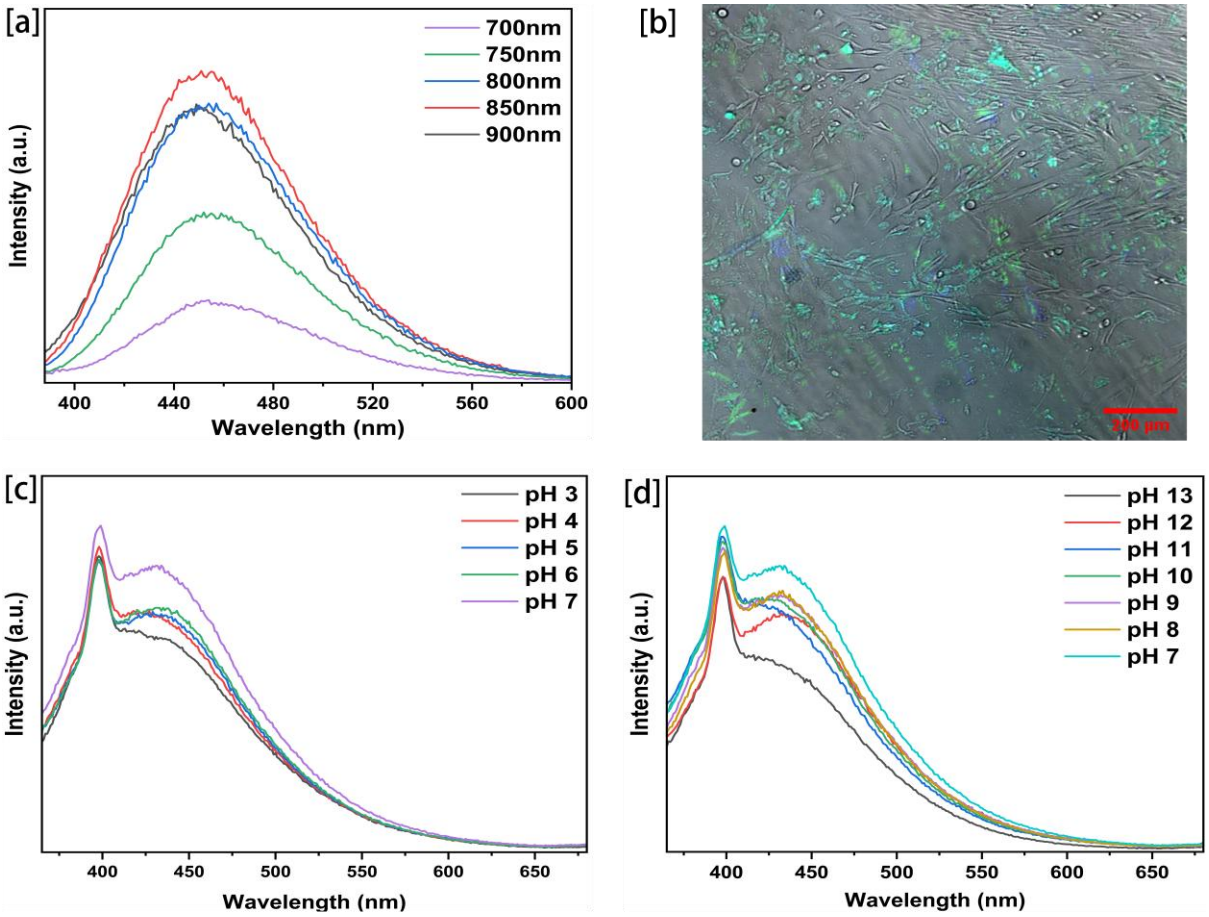

Figure 6. (a) The up-conversion emission spectra of GW CDs under different UV wavelengths. (b) The cell image of BJ5TA under 400 nm (blue light) and 488 nm (green light) after being exposed to GW CDs. (c)-(d) Fluorescence changes of GW CDs under different pH conditions under 350 nm UV light.

3. Conclusion

A novel amphiphilic and sustainable carbon dot (GW CD) was successfully synthesised via a microwave-assisted method using acrylic acid and gromwell root waste. GW CDs exhibited dual functionality as both Pickering emulsion stabilisers and photoinitiators, combining interfacial stabilisation with efficient radical generation under UV light. Their amphiphilic surface chemistry, featuring both hydrophobic and hydrophilic groups, enabled stable oil-in-water emulsions and effective interfacial adsorption. Upon UV irradiation, GW CDs generated carbon-centred, peroxyhydroxyl, and hydroxyl radicals, supporting their capacity to initiate free radical polymerisation.

In EHA, IBOA, and TMPTA-based high internal phase emulsions, GW CDs facilitated the formation of stable emulsions and crosslinked PolyHIPEs with larger pore sizes than those formed using conventional Hypermer and TPO systems. Notably, the pore architecture, including pore throat diameter and connectivity, could be tuned by adjusting the GW CDs concentration. At concentrations below 14 wt%, GW CDs-

based PolyHIPEs maintained superior pore throat dimensions and permeability, offering advantages for mass transport and cell infiltration.

In addition to their dual functionality, GW CDs demonstrated excellent pore improvement, supporting higher cell viability and normal morphology across multiple cell lines compared to traditional stabiliser and initiator systems. Furthermore, GW CDs exhibited unique properties such as upconversion photoluminescence, pH responsiveness, and intracellular fluorescence, highlighting their potential for broader applications in biomedical engineering, environmental remediation, and functional material design.

4. Experimental Section

4.1 Materials

Gromwell roots powder was purchased from Mystic Moments (Fordingbridge, UK), ethanol, limonene, dimethyl sulphoxide (DMSO), methanol, deuterium oxide (D_2O), 5,5-Dimethyl-1-pyrroline N-oxide (DMPO), 4-phenyl-2-tert-butyl nitrone (PBN), L-glutamine, amphotericin B, foetal bovine serum (FBS), penicillin/streptomycin (P/S), trypsin, paraformaldehyde, Phalloidin-TRITC, BJ-5TA cells, HaCaT cells, MLO-A5 cells, NG-108 cells were all purchased from Sigma-Aldrich (Darmstadt, Germany). 2-ethylhexyl acrylate (EHA), isobornyl acrylate (IBOA), trimethylolpropane triacrylate (TMPTA), 1 kDa dialysis membrane, acrylic acid, 2,4,6-Trimethylbenzoyldiphenylphosphine oxide (TPO), pyrene, quinine sulfate (QS), NaOH, HCl were purchased from Thermo Fisher Scientific Inc. (Waltham, MA, USA). Hypermer B246 was purchased from Croda International Plc. (New York, NY, USA) and deionized (DI) water.

4.2 Acquisition of GW

Groomwell root powder was extracted with 70% ethanol at a mass ratio of 1:10 at 80 °C for 2.5 hours, after which the insoluble residue was separated using filter paper [54]. This extraction process was repeated three times. The shikonin was dissolved in ethanol, while the remaining insoluble residues were collected and placed in a vacuum oven (Fistreem Vacuum Oven, Fistreem International Ltd, Cambridge, UK) at 30 mtorr, 60°C to remove residual ethanol, resulting in the production of Gromwell root powder waste (GW).

4.3 Synthesis of GW CDs

0.5 g of GW was thoroughly dispersed in 20 g of acrylic acid via ultrasonication (The

Fisher Scientific FB15051 ultrasonic baths, Thermo Fisher Scientific Inc., Waltham, MA, USA) and subsequently heated at 180 °C in microwave (CEM Discover® 2.0 (CEM Corporation, Matthews, NC, USA)) for 20 minutes to produce a viscous black liquid. The resulting liquid was transferred into a dialysis membrane with a 1 kDa molecular weight cut-off and dialyzed against deionized water to the complete removal of acrylic acid and other small molecule impurities. The aqueous solution was removed to remove the high-hydrophilic component, and the remaining precipitate was washed with limonene to remove the high-hydrophobic component. The left crude products were dissolved in 1:1 ethyl acetate/water solvent and then vacuum oven-dried (Fistreem Vacuum Oven (Fistreem International Ltd, Cambridge, UK)) to yield light grey flocculent GW CDs.

4.4 Synthesis of PolyHIPEs

42 wt% 2-ethylhexyl acrylate (EHA), 42 wt% 3-isobornyl acrylate (IBOA), 16 wt% trimethylolpropane triacrylate (TMPTA), and half amount of different proportions of GW CDs (1 wt%, 2 wt%, 4 wt%, 6 wt% until 14 wt%) were mixed, along with a control group formulated without CDs but containing all amount of 4 wt% Hypermer B246 and 4 wt% of TPO (Table S1) [55]. Finally, 80 vol% of deionized (DI) water mixed with the other half amount of GW CDs was added dropwise as the internal phase while stirring at 500 rpm using a SciQuip-Pro 40 stirrer (Rotherham, UK) to form stable emulsions (Top of Figure S1a). All emulsions were then cured under a 365 nm UV lamp (Dymax BlueWave® FX-1250 High Intensity LED UV Curing Flood Lamp (Dymax®, Wiesbaden, Germany), 1700 mW/cm^2) for 180s to obtain cross-linked PolyHIPEs (bottom of Figure S1a).

4.5 Characterizations

4.5.1 Transmission electron microscope (TEM)

The GW CDs before and after 365 nm UV irradiation with 600s were examined using a cold field emission (c-FEG) JEOL F200 TEM (JEOL Ltd., Tokyo, Japan) operating at 200 kV. The CA CDs methanol solution was evenly spread on the copper grid and air-dried to visualize the nano particles.

4.5.2 X-ray Diffraction Spectroscopy (XRD)

Panalytical Aeris X-ray Diffraction Spectroscopy (Malvern Panalytical Ltd, Malvern, UK) was used for XRD of GW CDs and GW CDs were exposed under 365nm UV light with 600s by setting the mode at 20min 10-80° scanning rotating. The CA CDs powder was carefully filled in the sample ring cavities.

4.5.3 Thermogravimetric Analysis (TGA)

10 mg of GW CDs were placed in the crucible of a PerkinElmer Pyris 1 TGA

instrument (Artisan Technology Group, Champaign, IL, USA) and heated from 30 °C to 600 °C at a rate of 10 °C/min to measure their mass change.

4.5.4 X-ray photoelectron spectroscopy (XPS)

X-ray photoelectron spectroscopy (XPS) was performed using Al Kα X-rays (1.486 keV photon energy, 20 mA emission at 300 W) in an Axis Ultra spectrometer (Kratos Analytica, Kyoto, Japan). The X-ray spot was approx. 1 mm diameter. Survey spectra were measured with pass energy 80 eV, and high-resolution core level spectra with 20 eV. Binding energy positions are compared to literature values, including databases from NIST, USA. GW CDs samples were pressed onto conductive copper tape using clean stainless-steel spatulas to create a uniform area ~15 mm diameter. Charge neutralization of powders and insulators is achieved using a low energy electron source in vacuum (PREVAC). The measurements were performed under ultra-high vacuum conditions with an instrument base pressure of approx. $1x10^{-8}$ mbar. Avantage software (Thermo Fisher Scientific Inc., Waltham, MA, USA) was used to deconvolute the peaks of different elements.

4.5.5 Attenuated total reflectance-fourier transform infrared (ATR-FTIR)

Attenuated total reflectance-Fourier transform infrared (ATR-FTIR) spectroscopy was conducted on GW CDs samples and the GW CDs were exposed under 365nm UV light with 60s, 120s, 180s, 300s and 600s via Perkin Elmer Frontier Fourier Transform Infrared (FTIR) (PerkinElmer, Waltham, MA, USA) with iD7 Single-Bounce ATR Accessories scanning between 600 and 4000 cm^{-1}.

The polymerization rate of the organic phase was also monitored by plotting conversion-time curves from time-resolved FTIR. The organic phase composition was identical to that used for emulsion fabrication and GW CDs 1-14 wt% and TPO were added at 2 or 5 wt% with respect to the total organic phase, respectively. UV exposure was conducted using a 405 nm wavelength lamp (M405L2 UV-mounted LED lamp (Thorlabs Inc., Newton, NJ, USA)) at an intensity of 700 mW/cm². Sequential spectra were acquired for 300s under continuous irradiation at 10-second intervals. Double-bond conversion was quantified by following the decrease of the characteristic C=C absorption band at ~810 cm^{-1} normalized to the carbonyl band (C=O) at ~1720 cm^{-1}, which was assumed to remain constant during curing:

$$\boldsymbol{Conversion}\ (\%) = \mathbf{1} - \left(\frac{\boldsymbol{A}_{\boldsymbol{C=C\ after\ exposure}}/\boldsymbol{A}_{\boldsymbol{C=O\ after\ exposure}}}{\boldsymbol{A}_{\boldsymbol{C=C\ before\ exposure}}/\boldsymbol{A}_{\boldsymbol{C=O\ before\ exposure}}}\right) \times \mathbf{100}\% \qquad (1)$$

where $A_{C=C}$ and $A_{C=O}$ are the C=C and C=O peak areas before and after exposure, respectively. Conversion-time curves were obtained for formulations containing 1-14 wt% GW CDs and for formulations containing 2 wt% and 5 wt% TPO.

4.5.6 Proton nuclear magnetic resonance (NMR) spectroscopy

The GW CDs were dispersed in 1% w/v. deuterated H_2O (D_2O) and use 400 MHz ^1H and ^{13}C nuclear magnetic resonance (NMR) (Burker AVIIIHD 400 NMR spectrometer (Blue Scientific Limited, Cambridge, UK)) to test. D_2O at 4.8 ppm in ^1H NMR spectrum is used as a chemical shift standard. D_2O shows no peak in ^{13}C NMR

spectrum. MestReNova software (MestreLab Research, Santiago de Compostela, Spain) was used to analyze the spectra. To calculate the hydrophilic-lipophilic balance (HLB) of the GW CDs, the peak between 1-1.15 ppm in the ^{1}H NMR spectrum was used as reference, and the peak areas in ^{1}H NMR spectrum were integrated. The HLB was then calculated using Griffin's empirical formula [56]:

$$HLB = 20 \cdot \frac{M_H}{M_T} \quad (2)$$

where M_H is the molecular mass of the hydrophilic portion of the molecule, and M_T is the molecular mass of the whole molecule.

4.5.7 UV-vis absorption spectroscopy (UV-vis)

Varian Cary 50 UV-vis absorption Spectrometer (Agilent, Santa Clara, CA, USA) was used for testing absorption properties of GW CDs in deionized water, with wavelength readings between 250 and 600 nm, scanning at a medium rate.

4.5.8 Photoluminescence (PL) spectroscopy

Horiba FluoroMax-4 Spectrofluorometer (HORIBA, Ltd., Kyoto, Japan) was used for testing excitation and emission spectra. Emission spectra of CA CDs aqua solutions were tested with excitation wavelengths under 345 nm, the scanning was at a medium rate. Up-conversion luminescence properties of GW CDs were evaluated at excitation wavelengths of 700 nm, 750 nm, 800 nm, 850 nm, and 900 nm; at 800 nm measurements the sample absorbance at the excitation wavelength was kept below 0.1, and excitation/emission slit widths, PMT voltage, and integration time were carefully controlled. Power-dependence tests were performed by varying the excitation slit width (1, 2, 4, 8, and 16 nm) at 800 nm while keeping all other parameters constant, and the emission intensity at the maximum was analyzed on a log-log scale. Excitation-Emission Matrix (EEM) of GW CDs were scanned with excitation and emission wavelengths between 250nm to 600nm and remove the Rayleigh and Raman scattering disturbing.

The photoluminescence quantum yield (PLQY) of the carbon dots was determined by comparing the fluorescence intensity of their aqueous solution with that of quinine sulfate (QS) (dissolved in 0.05 mol/L sulfuric acid, PLQY = 54%) as a reference, following the standard quantum yield calculation method [57]:

$$PLQY_{GW\ CDs} = PLQY_{QS} \frac{S_{GW\ CDs}}{S_{QS}} \cdot \frac{A_{QS}}{A_{GW\ CDs}} \cdot \frac{\eta^2_{GW\ CDs}}{\eta^2_{QS}} \quad (3)$$

where PLQY is photoluminescence quantum yield, QS represents the quinine-sulfate reference solution, S means the integral area of the fluorescence peak in the PL spectra, A expresses the absorbance at the excitation wavelength, and η represents the refractive index of the solution. The absorbance less than 0.1 can be regarded as the same refractive index.

The emission intensities of GW CDs (0.05 g/L) dispersed in water and in an EHA/IBOA/TMPTA prepolymer mixture (comprising 42% EHA, 42% IBOA, and 16% TMPTA) were also measured and compared under 350 nm excitation.

The critical micelle concentration (CMC) of GW CDs was determined based on

fluorescence intensity changes [58]. The GW CDs were dispersed into water and prepolymer mixture, where water constituted 80 vol%, and the prepolymer phase (comprising EHA, IBOA, and TMPTA) was prepared at a mass ratio of 42:42:16. GW CDs were added at varying concentrations, and the mixtures were ultrasonicated (The Fisher Scientific FB15051 ultrasonic baths, Thermo Fisher Scientific Inc., Waltham, MA, USA) for 5 minutes to ensure homogeneous dispersion. Immediately after mixing, fluorescence spectra were recorded with excitation at 350 nm, and the corresponding fluorescence peak areas were calculated.

To evaluate the pH sensitivity of GW CDs, solutions with pH values ranging from 3 to 13 were prepared by adding appropriate amounts of HCl or NaOH to deionized water. GW CDs were dispersed in these solutions at a concentration of 0.05 g/L. Fluorescence emission spectra were then recorded at an excitation wavelength of 350 nm.

To qualitatively investigate the interaction between GW CDs and prepolymer, steady-state PL quenching experiments were conducted. Fluorescence emission spectra were recorded for GW CDs and TPO, both dissolved in ethanol at fixed concentrations (0.25 mg/mL), under 365 nm excitation. The prepolymer mixture (EHA/IBOA/TMPTA = 42:42:16 by mass) was added incrementally (0, 5, 10, 20, 50, 100 mM), and absorbance was maintained ≤ 0.2 at all stages to minimize inner filter effects. At each concentration, the maximum emission intensity (I) was recorded and compared to the initial intensity (I_0) to construct Stern-Volmer plots, showing I_0/I as a function of monomer concentration. The Stern-Volmer constant (K_{SV}) was obtained from linear fitting to:

$$\frac{I_0}{I} = 1 + K_{SV}[Prepolymer] \quad (4)$$

4.5.9 Water contact angle test and liquid penetration test

Water contact angle test was performed using a Kruss DSA100 Optical Contact Angle Meter (KRÜSS, Bristol, UK) to measure the hydrophilicity of GW CDs which fully covered on the glass. A drop of 20 μL deionized water was loaded on sample surface and the drop shape image was taken and analysed using the software Drop Shape Analysis (KRÜSS, Bristol, UK).

The liquid penetration test was also performed by this machine, a drop of 20 μL deionized water was loaded on PolyHIPEs surface and record the time from the beginning of dropping to complete penetration inside the material. All tests were repeated three times for each sample.

4.5.10 Electron Paramagnetic Resonance (EPR)

Electron Paramagnetic Resonance (EPR) experiments were carried out using a ELEXSYS-II E500T (X-band) spectrometer at 100 kHz equipped with Bruker ELEXSYS Super High Sensitivity Probehead. The power intensity was adjusted to 20 mW. The radicals of GW CDs in deionized water and deoxygenated water were generated through photolysis at room temperature when exposed to the 365 nm UV (24 mW/cm^2) with DMPO. The EPR spectra simulations were performed using the

Easyspin. Deoxygenated water was prepared by boiling deionized water and then purging with Nitrogen for 20-40 minutes at a flow rate of 25 mL/s.

4.5.11 Cell viability test

BJ-5TA (P22-26), HaCaT (P83-89), MLO-A5 (P49-55), NG-108 (P11-15) cells were revived from -80 °C cryovial stocks. The culture media was based on Dulbecco's modified Eagle's medium (DMEM) and was supplemented with 10% v/v FBS, 1% v/v L-glutamine, P/S and 1% v/v amphotericin B. The cells were incubated at 37°C, 5% CO_2 and were passaged when their confluency under light microscope reached 70% - 80%. Cells were seeded in 48-well plates at the density of 1×10^4 cells per well.

The cell metabolic activity on the samples was measured via resazurin reduction assay and seeding on TCP as positive control. The resazurin sodium salt was dissolved in PBS in the concentration of 25 mg/100 mL as the master stock and was diluted 10 times in culture media as reaction solution. The four cell lines were seeded into wells and initially incubated in media for 24 hours to allow for cell attachment. The media were then replaced with media containing 1 mg/mL GW CDs and 1 mg/mL Hypermer/TPO (0.5 mg/mL Hypermer + 0.5 mg/mL TPO) and incubated in the dark at 37 °C for an additional 24 hours. Following incubation, 200 µL of the solution from each well was transferred into a 96-well plate, and fluorescence was measured using a microplate reader (FLX800, BIO-TEK Instruments, Inc., Agilent, Santa Clara, CA, USA) at an excitation wavelength of 540 nm and an emission wavelength of 630 nm. All incubated cells were also taken under an optical microscope at 10× magnification to observe the cell morphology.

4.5.12 Scanning electron microscope (SEM)

All the PolyHIPEs were 5 nm gold-coated (Quorum Q150RS plus, Quorum Technologies Ltd., Lewes, UK) and evaluated by FEI Nova NanoSEM 450 (Field Electron and Ion Company, Hillsboro, OR, USA) at 5KV. Based on the SEM images, ImageJ software was used to quantify and calculate the average pore size, the average number of pore throats per pore, and the average pore throat diameter for each PolyHIPE sample. For each formulation, images from at least three different regions were analysed and 100 pores and 100 pore throats were measured to determine the average pore diameter, the average number of throats per pore and the average pore-throat diameter. All values are reported as mean ± standard deviation (n = 100). High-magnification images (4000×) were used to observe and compare the microscopic surface morphology of 5% Hypermer/TPO-PolyHIPE and 14 wt% GW CDs-PolyHIPE.

4.5.13 PolyHIPEs emulsion stability time before creaming and long-term emulsion stability test.

The stability time of each emulsion **before creaming** was recorded as the point at which visible creaming was first observed (Figure S1b). The long-term storage stability of GW CDs-stabilized emulsions was evaluated by monitoring changes in droplet size over time using optical microscopy. The emulsions were prepared following the

method described in Experimental Section 4.3. Immediately after emulsification, a small amount of freshly prepared emulsion was gently transferred onto a glass slide, covered with coverslip, and imaged without disturbing the droplet structure. Bright-field images were acquired at room temperature (20 °C) using an optical microscope (AE2000 Inverted Microscopes, Motic, Hong Kong, China) equipped with a digital camera and 10× objectives. These images correspond to time zero (t = 0). The remaining emulsion sample was stored in sealed vials at 20 °C and resampled at predefined time points: 30 minutes, 1 hour, 2 hours, 4 hours, 8 hours, 1 day, and 7 days. At each point, a small amount of emulsion was transferred onto a glass slide and imaged under the same conditions. For each formulation and time point, at least 100 droplets were analyzed from multiple randomly selected fields of view using ImageJ software. The equivalent circular diameter of each droplet was calculated based on its projected area, and the average droplet diameter along with the standard deviation was determined.

4.5.14 Static light scattering (SLS) measurement

Static light scattering (SLS) was employed to measure the droplet size distribution of emulsions stabilized with varying concentrations of GW CDs at different temperatures (20 °C, 45 °C, and 70 °C). Emulsions were incubated in a constant-temperature oven until equilibrium was reached. The droplet diameter distribution was determined using a Malvern Mastersizer 2000 (Malvern Instruments Ltd., Malvern, Worcestershire, UK) equipped with a 633 nm He-Ne laser and a 466 nm solid-state blue laser. The average droplet diameter is calculated from the diameter distribution.

4.5.15 Surface temperature test of PolyHIPEs after curing

The surface temperature of GW CDs-stabilized PolyHIPEs was measured immediately after 180 seconds of UV curing (under a 365nm UV lamp (Dymax BlueWave® FX-1250 High Intensity LED UV Curing Flood Lamp (Dymax®, Wiesbaden, Germany), 1,700 mW/cm^2)) using a WIGGENS PT100-01 temperature sensor (WIGGENS GmbH, Germany). Each sample was measured in triplicate.

4.5.16 Confocal imaging

To determine the location of GW CDs in PolyHIPE, cross-sections of 1-14 wt% GW CDs-polyHIPE were directly imaged using Nikon A1 confocal microscope (Nikon, Tokyo, Japan) with an excitation wavelength of 488 nm (Alexa Fluor 488). To assess the cell imaging capability of GW CDs, BJ- 5TA cells were seeded at a density of 10,000 cells per well in 48-well culture plates. The cells were initially cultured in the media for 24 hours to settle down, and the cells were fed with media supplemented with 1 mg/mL GW CDs every two days. On day 7, the cells were removed media and directly imaged using the confocal microscope under excitation wavelength of 488 nm (Alexa Fluor 488) and 400nm (DAPI).

The Hypermer/TPO-PolyHIPE and 10 wt% GW CDs-PolyHIPE scaffolds were cut

into 1 mm thick discs (d = 8 mm). The sample discs were sterilized in 70% ethanol for 1 h and dried under UV for 30 min on both sides. 5×10^3 MDA-MB-231 cells with GFP (Green Fluorescent Protein) marked were seeded on the surface each scaffold and were cultured in DMEM (supplemented with 10 % FBS, 1% P/S, 1% F and 1% L-Glutamine by volume) at 37 °C, 5% CO_2 atmosphere. The media changed every two days. On day 7, cells on the scaffolds were fixed in 3.7% paraformaldehyde (PFA) and the cytoskeleton was stained red by Phalloidin-TRITC. The scaffolds were observed under blue light (wavelength 405 nm), green light (wavelength 488 nm) and red light (wavelength 562 nm) using Nikon A1 confocal microscope.

4.5.17 Statistical analysis

Differences between groups were assessed using GraphPad Prism one-way Analysis of Variance (ANOVA) test for cell viability test, and the results were plotted as mean ± standard deviation (SD). Significant differences between each experimental group were analyzed. Significant difference was defined as *p < 0.05. Highly significant differences were defined as **p < 0.01, ***p < 0.001, and ****p < 0.0001.

4.5.18 Photo-DSC measurements

The analysis was conducted using a Pyris Diamond DSC 6 (PerkinElmer, Shelton, CT, USA). A M405L2 UV-mounted LED lamp (Thorlabs Inc., Newton, NJ, USA; 405 nm, 700 mW/cm^2) was mounted 1 cm above the open sample chamber. Approximately 5 mg of prepolymer sample (IBOA/EHA/TMPTA, with GW CDs or TPO at the same concentrations as in the FTIR polymerization rate experiments) was placed in an aluminium DSC pan. The reference was an empty pan. All measurements were performed at 30 °C under a nitrogen atmosphere (20 mL/ min). The UV light source was controlled via a Thorlabs development controller and triggered after a 1-second temperature equilibration. Samples were irradiated for 10 mins, and the resulting heat flow was continuously recorded. The heat-flow curves (mW/g) were integrated to obtain the total reaction enthalpy (ΔH, J/g).

4.5.19 Vials inversion test

The curing efficiency of GW CDs was evaluated by a vial inversion method combined with gel-fraction analysis. Emulsions were prepared by mixing the organic phase (42 wt% IBOA, 42 wt% EHA, 16 wt% TMPTA with 1-14 wt% GW CDs, or with 2 or 5 wt% TPO) with deionized water as internal phase. The water volume fraction was fixed at 80 vol% in all cases. For the vial inversion test, approximately 2.0 g of each freshly prepared emulsion was transferred into 10 mL glass beakers (n = 3 for each composition). Vials were placed under a M405L2 UV-mounted LED lamp (Thorlabs Inc., Newton, NJ, USA; 405 nm, 700 mW/cm²) at a 5 cm distance of the sample surface. Immediately after the UV lamp was switched on, the vials were tilted at regular intervals of 5 s. The gelation time (t_{gel}) was defined as the time at which the emulsion no longer flowed upon tilting (Figure S14). To determine the gel fraction at the gel point, additional vials were prepared and irradiated for the respective tgel determined for each formulation. The cured PolyHIPEs were removed from the vials, cut into small pieces, and extracted with an excess of DMSO for 24 h to remove the soluble fraction. The samples were then dried to constant mass at 40 °C under vacuum.

The gel fraction (G) was calculated as:

$$\boldsymbol{G}(\%) = \frac{\boldsymbol{m_{dry}}}{\boldsymbol{m_{organic}}} \times \mathbf{100}\% \quad (5)$$

where m_{dry} is the mass after extraction and drying and $m_{organic}$ is the initial mass of the organic phase in the sample, calculated from its total mass and organic-phase weight fraction in the formulation. Gelation time and gel fraction are reported as mean ± standard deviation for three independent samples.

Acknowledgements

The authors acknowledge the financial assistance provided to Woming Gao, Zeming Cheng by the University of Sheffield. The authors would like to thank the Engineering and Physical Sciences Research Council (EPSRC) for funding EP/V012126/1 to Cornelia Rodenburg and Nicholas Farr. Frederik Claeyssens also thanks the Royal Society for funding a Royal Society Leverhulme Trust Senior Research Fellowship 2022 (SRF\R1\221053). Confocal imaging work was performed at the Wolfson Optical Microscopy Facility, and TEM (with thanks to Jiahui Qi) and SEM work was performed at Sorby Centre for Electron Microscopy. We thank Khalid Doudin for helping with measuring the NMR data. We also wish to acknowledge the support of the Henry Royce Institute for XPS test at University of Manchester. This work was supported by the Henry Royce Institute for Advanced Materials, funded through EPSRC grants EP/R00661X/1, EP/S019367/1, EP/P025021/1 and EP/P025498/1. We wish to acknowledge the support of the Henry Royce Institute for Advanced Materials at Imperial College London (with thanks to Irena Nevjestic), as well as access to SPIN-Lab Bruker X-band EPR spectrometer at Royce Imperial funded through EPSRC grants EP/P030548/1, EP/R00661X/1 and EP/P02520X/1.

Conflict of Interest

The authors declare no conflict of interest.

Data Availability Statement

The data that support the findings of this study are available from the corresponding author upon reasonable request.

References

[1] N. Sengokmen-Ozsoz, R. Boston, J. S. Dean, C. Rodenburg, and F. Claeyssens, 'Fabrication of hierarchically porous carbon lattices derived from 3D-Printed polymerized high internal phase emulsions', *Carbon*, vol. 234, p. 119933, Mar. 2025, doi: 10.1016/j.carbon.2024.119933.

[2] B. Aldemir Dikici and F. Claeyssens, 'Basic Principles of Emulsion Templating and Its Use as an Emerging Manufacturing Method of Tissue Engineering Scaffolds', *Front. Bioeng. Biotechnol.*, vol. 8, p.875, Aug. 2020, doi: 10.3389/fbioe.2020.00875.

[3] S. J. Pierre *et al.*, 'Covalent Enzyme Immobilization onto Photopolymerized Highly Porous Monoliths', *Adv. Mater.*, vol. 18, pp. 1822-1826, Jul. 2006, doi: 10.1002/adma.200600293.

[4] R. Owen, C. Sherborne, T. Paterson, N. H. Green, G. C. Reilly, and F. Claeyssens, 'Emulsion templated scaffolds with tunable mechanical properties for bone tissue engineering', *J. Mech. Behav. Biomed. Mater.*, vol. 54, pp. 159–172, Feb. 2016, doi: 10.1016/j.jmbbm.2015.09.019.

[5] H. Bahmaee *et al.*, 'Design and Evaluation of an Osteogenesis-on-a-Chip Microfluidic Device Incorporating 3D Cell Culture', *Front. Bioeng. Biotechnol.*, vol. 8, p.557111, Sep. 2020, doi: 10.3389/fbioe.2020.557111.

[6] S. Rebello, A. K. Asok, S. Mundayoor, and M. S. Jisha, 'Surfactants: toxicity, remediation and green surfactants', *Environ. Chem. Lett.*, vol. 12, pp. 275-287, Jun. 2014, doi: 10.1007/s10311-014-0466-2.

[7] X. Ji *et al.*, 'Occurrence, Fate, Human Exposure, and Toxicity of Commercial Photoinitiators', *Environ. Sci. Technol.*, vol. 57, pp. 11704–11717, Aug. 2023, doi: 10.1021/acs.est.3c02857.

[8] S. Rebello, A. K. Asok, S. Mundayoor, and M. S. Jisha, 'Surfactants: Chemistry, Toxicity and Remediation', in *Pollutant Diseases, Remediation and Recycling*, E. Lichtfouse, J. Schwarzbauer, and D. Robert, Eds., Cham, Switzerland: Springer International Publishing, 2013, pp. 277–320. doi: 10.1007/978-3-319-02387-8_5.

[9] B. Zeng *et al.*, 'Cytotoxic and cytocompatible comparison among seven photoinitiators-triggered polymers in different tissue cells', *Toxicol. In Vitro*, vol. 72, p. 105103, Apr. 2021, doi: 10.1016/j.tiv.2021.105103.

[10] G. C. J. Lindberg *et al.*, 'Biological function following radical photo-polymerization of biomedical polymers and surrounding tissues: Design considerations and cellular risk factors', *Appl. Phys. Rev.*, vol. 8, p. 011301, Jan. 2021, doi: 10.1063/5.0015093.

[11] H. Refaat *et al.*, 'Challenges with effective removal of surfactants from monoclonal antibody formulations', *Int. J. Pharm.*, vol. 670, p. 125146, Feb. 2025, doi: 10.1016/j.ijpharm.2024.125146.

[12] L. Xu, N. Sheybani, W. A. Yeudall, and H. Yang, 'The effect of photoinitiators on intracellular AKT signaling pathway in tissue engineering application', *Biomater. Sci.*, vol. 3, pp. 250-255, Jan. 2015, doi: 10.1039/C4BM00245H.

[13] V. O. Ikem, A. Menner, and A. Bismarck, 'Tailoring the mechanical performance of highly permeable macroporous polymers synthesized via Pickering emulsion templating', *Soft Matter*, vol. 7, pp. 6571-6577, Jul. 2011, doi: 10.1039/C1SM05272A.

[14] W. Gao *et al.*, 'Advancing synthetic bone tissue engineering materials: Nano-scale investigation into transitional Interface in carbon dots/ polymer composites', *J. Colloid Interface Sci.*, vol. 700, p. 138553, Dec. 2025, doi: 10.1016/j.jcis.2025.138553.

[15] R. Lu, S. He, T. Wang, L. Lai, and M. Zhao, 'Low-cost preparation of temperature-resistant and

salt-tolerant amphiphilic carbon dots from a nonionic surfactant and its application in enhanced oil recovery', *Carbon*, vol. 225, p. 119104, May 2024, doi: 10.1016/j.carbon.2024.119104.
[16] Y. Cheng et al., 'N-doped carbon dots-modulated interfacial charge transfer and surface structure in $FeNbO_4$ photocatalysts for enhanced CO_2 conversion selectivity to CH_4', *Chem. Eng. J.*, vol. 498, p. 155576, Oct. 2024, doi: 10.1016/j.cej.2024.155576.
[17] Y.-S. Seo and J.-W. Kang, 'Synthesis and characterization of clove residue-derived carbon quantum dots: Application in Pickering emulsion with enhanced antibacterial properties', *Chem. Eng. J.*, vol. 503, p. 158247, Jan. 2025, doi: 10.1016/j.cej.2024.158247.
[18] Y. Wang *et al.*, 'Preparation of surface-active carbon dots with fluorocarbon and hydrocarbon hybrid chains via a one-pot solvothermal technique and their characterization and potential applications', *Colloids Surf. Physicochem. Eng. Asp.*, vol. 684, p. 133155, Mar. 2024, doi: 10.1016/j.colsurfa.2024.133155.
[19] R. Li *et al.*, 'Type I Photoinitiator Based on Sustainable Carbon Dots', *Angew. Chem. Int. Ed.*, vol. 63, p. e202404454, Apr. 2024, doi: 10.1002/anie.202404454.
[20] K. Chang, Q. Zhu, L. Qi, M. Guo, W. Gao, and Q. Gao, 'Synthesis and Properties of Nitrogen-Doped Carbon Quantum Dots Using Lactic Acid as Carbon Source', *Materials*, vol. 15, p. 466, Jan. 2022, doi: 10.3390/ma15020466.
[21] R. Ma, M. Zeng, D. Huang, J. Wang, Z. Cheng, and Q. Wang, 'Amphiphilicity-adaptable graphene quantum dots to stabilize pH-responsive pickering emulsions at a very low concentration', *J. Colloid Interface Sci.*, vol. 601, pp. 106-113, Nov. 2021, doi: 10.1016/j.jcis.2021.05.104.
[22] E. Durgut, M. Zhou, B. A. Dikici, R. Foudazi, and F. Claeyssens, 'Modifying pickering polymerized high internal phase emulsion morphology by adjusting particle hydrophilicity', *Colloids Surf. Physicochem. Eng. Asp.*, vol. 680, p. 132629, Jan. 2024, doi: 10.1016/j.colsurfa.2023.132629.
[23] D. Yi, G. Jeong, J.-H. Seo, M. J. Yoo, and H. Yang, 'Carbon Dots with Tailored Surface Wettability as Pickering Emulsifiers', *ACS Appl. Nano Mater.*, vol. 5, pp. 10258–10267, Aug. 2022, doi: 10.1021/acsanm.2c01277.
[24] B. Wang *et al.*, 'Rational Design of Multi-Color-Emissive Carbon Dots in a Single Reaction System by Hydrothermal', *Adv. Sci.*, vol. 8, p. 2001453, Nov. 2021, doi: 10.1002/advs.202001453.
[25] W. Li *et al.*, 'Carbon-Quantum-Dots-Loaded Ruthenium Nanoparticles as an Efficient Electrocatalyst for Hydrogen Production in Alkaline Media', *Adv. Mater.*, vol. 30, p. 1800676, Jul. 2018, doi: 10.1002/adma.201800676.
[26] H. Yang *et al.*, 'Hydrophobic carbon dots with blue dispersed emission and red aggregation-induced emission', *Nat. Commun.*, vol. 10, p. 1789, Apr. 2019, doi: 10.1038/s41467-019-09830-6.
[27] A. Mewada *et al.*, 'Green synthesis of biocompatible carbon dots using aqueous extract of *Trapa bispinosa* peel', *Mater. Sci. Eng. C*, vol. 33, pp. 2914-2917, Jul. 2013, doi: 10.1016/j.msec.2013.03.018.
[28] Preeti *et al.*, 'Nanoemulsion: An Emerging Novel Technology for Improving the Bioavailability of Drugs', *Scientifica*, vol. 2023, p. 6640103, Oct. 2023, doi: 10.1155/2023/6640103.
[29] M. Mieles, S. Harper, and H.-F. Ji, 'Bulk Polymerization of Acrylic Acid Using Dielectric-Barrier Discharge Plasma in a Mesoporous Material', *Polymers*, vol. 15, p. 13, Jan. 2023, doi: 10.3390/polym15132965.
[30] F.-M. Yin *et al.*, 'Unconventional Fluorescent and Multi-responsive Polyethyleneimine with LCST and UCST Behavior: Synthesis, Characterization and Biological Applications', *Chin. J. Polym. Sci.*,

vol. 42, pp. 826-837, Jun. 2024, doi: 10.1007/s10118-024-3120-x.
[31] X. Zhuang, J. Liu, C. Wang, Q. Zhang, and L. Ma, 'Microwave-assisted hydrothermal liquefaction for biomass valorization: Insights into the fuel properties of biocrude and its liquefaction mechanism', *Fuel*, vol. 317, p. 123462, Jun. 2022, doi: 10.1016/j.fuel.2022.123462.
[32] S. Z. N. Ahmad, W. N. Wan Salleh, A. F. Ismail, N. Yusof, M. Z. Mohd Yusop, and F. Aziz, 'Adsorptive removal of heavy metal ions using graphene-based nanomaterials: Toxicity, roles of functional groups and mechanisms', *Chemosphere*, vol. 248, p. 126008, Jun. 2020, doi: 10.1016/j.chemosphere.2020.126008.
[33] F. Dai, Q. Zhuang, G. Huang, H. Deng, and X. Zhang, 'Infrared Spectrum Characteristics and Quantification of OH Groups in Coal', *ACS Omega*, vol. 8, pp. 17064-17076, May 2023, doi: 10.1021/acsomega.3c01336.
[34] I. Y. Miranda-Valdez *et al.*, 'Bio-Based Foams to Function as Future Plastic Substitutes by Biomimicry: Inducing Hydrophobicity with Lignin', *Adv. Eng. Mater.*, vol. 26, p. 2400233, Aug. 2024, doi: 10.1002/adem.202400233.
[35] Jim Clark, 'Interpreting C-13 NMR spectra?', Chemguide. Accessed: Apr. 26, 2025. [Online]. Available: https://www.chemguide.co.uk/analysis/nmr/interpretc13.html
[36] B. Zhao *et al.*, 'Triphenylamine-Derived Solid-State Emissive Carbon Dots for Multicolor High-Efficiency Electroluminescent Light-Emitting Diodes', *Angew. Chem.*, vol. 135, p. e202301651, Mar. 2023, doi: 10.1002/ange.202301651.
[37] J. Wu, F. Yan, Q. Jia, and Q. Wang, 'QSPR for predicting the hydrophile-lipophile balance (*HLB*) of non-ionic surfactants', *Colloids Surf. Physicochem. Eng. Asp.*, vol. 611, p. 125812, Feb. 2021, doi: 10.1016/j.colsurfa.2020.125812.
[38] S. M. Rahaman, A. Bhattarai, D. Kumar, B. Singh, and B. Saha, 'Chapter 11 - Application of biosurfactants as emulsifiers in the processing of food products with diverse utilization in the baked goods', in *Applications of Next Generation Biosurfactants in the Food Sector*, Inamuddin and C. O. Adetunji, Eds., Amsterdam, Netherlands: Academic Press, 2023, pp. 203-237. doi: 10.1016/B978-0-12-824283-4.00021-6.
[39] M. Sbacchi, M. Mamone, L. Morbiato, P. Gobbo, G. Filippini, and M. Prato, 'Shining Light on Carbon Dots: New Opportunities in Photocatalysis', *ChemCatChem*, vol. 15, p. e202300667, Jun. 2023, doi: 10.1002/cctc.202300667.
[40] S. Bhattacharyya *et al.*, 'Effect of nitrogen atom positioning on the trade-off between emissive and photocatalytic properties of carbon dots', *Nat. Commun.*, vol. 8, p. 1401, Nov. 2017, doi: 10.1038/s41467-017-01463-x.
[41] Y. Huang, L. Luo, S. Zhu, K. Yin, L. Bu, and S. Zhou, 'Revealing the crucial role of Carbon-Centered radicals in UV/PAA process for trace amounts of organic contaminants removal', *Chem. Eng. J.*, vol. 475, p. 146254, Nov. 2023, doi: 10.1016/j.cej.2023.146254.
[42] M. Danilczuk, F. D. Coms, and S. Schlick, 'Visualizing Chemical Reactions and Crossover Processes in a Fuel Cell Inserted in the ESR Resonator: Detection by Spin Trapping of Oxygen Radicals, Nafion-Derived Fragments, and Hydrogen and Deuterium Atoms', *J. Phys. Chem. B*, vol. 113, pp. 8031-8042, Jun. 2009, doi: 10.1021/jp901597f.
[43] F. A. Villamena, E. J. Locigno, A. Rockenbauer, C. M. Hadad, and J. L. Zweier, 'Theoretical and Experimental Studies of the Spin Trapping of Inorganic Radicals by 5,5-Dimethyl-1-Pyrroline N-Oxide (DMPO). 1. Carbon Dioxide Radical Anion', *J. Phys. Chem. A*, vol. 110, pp. 13253-13258, Dec. 2006, doi: 10.1021/jp064892m.

[44] L. Y. Zang and H. P. Misra, 'EPR kinetic studies of superoxide radicals generated during the autoxidation of 1-methyl-4-phenyl-2,3-dihydropyridinium, a bioactivated intermediate of parkinsonian-inducing neurotoxin 1-methyl-4-phenyl-1,2,3,6-tetrahydropyridine.', *J. Biol. Chem.*, vol. 267, pp. 23601-23608, Nov. 1992, doi: 10.1016/S0021-9258(18)35881-2.

[45] S. González and X. Jaramillo-Fierro, 'Density Functional Theory Study of Methylene Blue Demethylation as a Key Step in Degradation Mediated by Reactive Oxygen Species', *Int. J. Mol. Sci.*, vol. 26, p. 1756, Feb. 2025, doi: 10.3390/ijms26041756.

[46] H. Tong *et al.*, 'Hydroxyl radicals from secondary organic aerosol decomposition in water', *Atmospheric Chem. Phys.*, vol. 16, pp. 1761-1771, Feb. 2016, doi: 10.5194/acp-16-1761-2016.

[47] D. Panda and J. Barik, 'Flooding Tolerance in Rice: Focus on Mechanisms and Approaches', *Rice Sci.*, vol. 28, pp. 43-57, Jan. 2021, doi: 10.1016/j.rsci.2020.11.006.

[48] J.-C. Brosse, D. Derouet, F. Epaillard, J.-C. Soutif, G. Legeay, and K. Dušek, 'Hydroxyl-terminated polymers obtained by free radical polymerization — Synthesis, characterization, and applications', in *Catalytical and Radical Polymerization*, Berlin, Heidelberg: Springer, 1986, pp. 167–223. doi: 10.1007/BFb0037615.

[49] Hydrogen Link, 'Hydroxyl Radicals Reactivity', Hydrogen Link Inc. Accessed: Jun. 23, 2025. [Online]. Available: https://www.hydrogenlink.com/hydroxylradicalsreactivity.

[50] P. Thangaraju and S. B. Varthya, 'ISO 10993: Biological Evaluation of Medical Devices', in *Medical Device Guidelines and Regulations Handbook*, P. S. Timiri Shanmugam, P. Thangaraju, N. Palani, and T. Sampath, Eds., Cham, Switzerland: Springer International Publishing, 2022, pp. 163-187. doi: 10.1007/978-3-030-91855-2_11.

[51] Y. Jiao *et al.*, 'Enhancing the Formation and Stability of Oil-In-Water Emulsions Prepared by Microchannels Using Mixed Protein Emulsifiers', *Front. Nutr.*, vol. 9, p. 822053, May 2022, doi: 10.3389/fnut.2022.822053.

[52] E. Durgut, C. Sherborne, B. Aldemir Dikici, G. C. Reilly, and F. Claeyssens, 'Preparation of Interconnected Pickering Polymerized High Internal Phase Emulsions by Arrested Coalescence', *Langmuir*, vol. 38, pp. 10953–10962, Sep. 2022, doi: 10.1021/acs.langmuir.2c01243.

[53] H. Li et al., 'Water-Soluble Fluorescent Carbon Quantum Dots and Photocatalyst Design', Angew. Chem., vol. 122, pp. 4532-4536, Jun. 2010, doi: 10.1002/ange.200906154.

[54] Y. H. Choi *et al.*, 'Ethanol extract of Lithospermum erythrorhizon Sieb. et Zucc. promotes osteoblastogenesis through the regulation of Runx2 and Osterix', *Int. J. Mol. Med.*, vol. 38, pp. 610-618, Aug. 2016, doi: 10.3892/ijmm.2016.2655.

[55] N. Sengokmen-Ozsoz, R. Boston, and F. Claeyssens, 'Investigating the Potential of Electroless Nickel Plating for Fabricating Ultra-Porous Metal-Based Lattice Structures Using PolyHIPE Templates', *ACS Appl. Mater. Interfaces*, vol. 15, pp. 30769-30779, Jun. 2023, doi: 10.1021/acsami.3c04637.

[56] K. Shinoda, H. Saito, and H. Arai, 'The effect of the size and the distribution of the oxyethylene chain lengths of nonionic emulsifiers on the stability of emulsions', *J. Colloid Interface Sci.*, vol. 35, pp. 624-630, Apr. 1971, doi: 10.1016/0021-9797(71)90220-7.

[57] S. Zhao, X. Chen, C. Zhang, P. Zhao, A. J. Ragauskas, and X. Song, 'Fluorescence Enhancement of Lignin-Based Carbon Quantum Dots by Concentration-Dependent and Electron-Donating Substituent Synergy and Their Cell Imaging Applications', *ACS Appl. Mater. Interfaces*, vol. 13, pp. 61565-61577, Dec. 2021, doi: 10.1021/acsami.1c20648.

[58] Y. Yang, M. Zhao, and L. Lai, 'Surface activity, micellization, and application of nano-

surfactants—amphiphilic carbon dots', *Carbon*, vol. 202, pp. 398-413, Jan. 2023, doi: 10.1016/j.carbon.2022.11.012.